Celal Bayar University Journal of Science
Volume 14, Issue 2, p 187-193

Synthesis and Characterization and Thermal Decomposition Kinetics of Poly (quinoline)-Copper Composite

Ali Bilici[1], Ruhiye Nilay Tezel[2], İsmet Kaya[1], Fatih Doğan[3*]

[1]Department of Chemistry, Faculty of Sciences and Arts, Çanakkale Onsekiz Mart University, 17020, Çanakkale, Turkey alibilici66@hotmail.com; ikaya@hotmail.com
[2]Lapseki Vocational School, Çanakkale Onsekiz Mart University, 17020, Lapseki, Çanakkale, Turkey nilaytezel@comu.edu.tr
[3]Secondary Science and Mathematics Education, Faculty of Education, Çanakkale Onsekiz Mart University, 17100, Çanakkale, Turkey *fatihdogan@comu.edu.tr

Received: 9 February 2018
Accepted: 15 May 2018
DOI: 10.18466/cbayarfbe.393015

Abstract

In here, chemical oxidative synthesis of a new poly(quinoline)-copper composite was given in one-step pathway. To obtain composite, the copper sulphate and 2-amino-8-quinolinol were used as oxidant and monomer, respectively. The oxidation product obtained was characterized by FTIR, UV-Vis, thermogravimetry (TG), photoluminescence (PL), SEM-EDX, TEM analysis and solid state conductivity measurements. SEM observations exhibited the presence of a plate-like heterogeneous morphology. Rod like structures was revealed from TEM images. TEM studies also indicated that the copper nanoparticles were almost uniformly distributed on polymer. The thermal decomposition kinetics of oxidation product were also studied. For this, the different methods such as Coats-Redfern, Flynn-Wall-Ozawa, Tang and Kissinger-Akahira-Sunose were used.

Keywords: Oxidative Polymerization, Composite, Quinoline, Thermal Analysis, Decomposition Kinetic.

1. Introduction

After the work of Stille and his colleagues [1], many studies have been performed for synthesis, characterization and different applications of polyquinolines [2]. Their high thermal and mechanical stability, low dielectric constant and interesting optical, electrical nature make these polymers the focus of attention [2]. Due to these properties, they have a wide range of usage including OLED, organic photovoltaic and chemosensor applications [2, 3]. The Freandliar reaction, Pd-catalyzed coupling reaction as well as chemical and electrochemical oxidation techniques are well-known methods for production of these polymers [2,4]. Chemical oxidation is one of the effective protocols to obtain polyaromatics. The procedure is simple and reactions are often performed out in ambient conditions. Besides, the high degree of conversion can be achieved [5]. To date, some quinoline composite materials have been prepared by chemical oxidation. For example, the composites of 3-amino quinoline [6, 7], 5-amino quinoline [8] and 6-amino quinoline [9] were prepared by using palladium, gold and copper salts, respectively.

In here, the preparation and characterization of new quinoline based composite (AQP/Cu) were presented. For this, 2-amino-8-quinolinol (AQ) was used as monomer and copper sulphate solution was used as oxidant. The physical and chemical characterizations of oxidation product were given. The thermal decomposition kinetics of AQP/Cu were also investigated.

2. Materials and Methods

2.1. Materials

The solvents and chemicals (analytical grade) used in this study were supplied from Sigma Chemical Company and used as received. A stock solution used in the synthesis was prepared by dissolving 1.33 g $CuSO_4.5H_2O$ in 100 mL methanol.

2.2. Synthesis of AQP/Cu

The previous work was followed for the synthesis of AQP/Cu [10]. For this, at first, methanol solution of monomer was prepared (0.2 g/10 mL) and then a stock solution (1 mL) was added to monomer solution drop by drop. Throughout the oxidant addition, the yellow colored solution turned into green, gradually and turbidity was observed. The resulting precipitates were gathered at the bottom of reaction flask. After filtration, the precipitates obtained were washed with distilled water and dried on vacuum oven.

2.3. Characterization techniques

Perkin Elmer FT-IR Spectrum One and Perkin Elmer Lambda 25 were used for FTIR and UV–Vis analysis, respectively. Perkin Elmer Diamond Thermal Analysis was used for thermal analysis (between 15º- 1000 °C, in

N_2, rate 5-20 °C min^{-1}). The fluorescent measurements were conducted using Schimadzu RF-5301PC spectrofluorophotometer (slit width: 5nm). JEOL JSM-7100F Schottky field emission SEM instrument was used to acquire the surface morphology of AQP/Cu. TEM images were acquired by using a JEOL TEM-1400 Plus microscope. Methanol was used for suspension of AQP/Cu and then it was dispersed, ultrasonically. The measurements were recorded using this suspension prepared (2mL). Solid state electrical conductivity of AQP/Cu was measured using a Keithley 2400 electrometer, in the pellet form. For this, powdery sample was exposed to a hydraulic press up to 1680 kg cm^{-2} and then pellet obtained was exposed to iodine vapors at atmospheric pressure in a desiccator at room temperature [9].

3. Results and Discussion

AQ is a derivate compound of 3-aminoquinoline (3AQ) and 6-aminoquinoline (6AQ). The oxidation of 3AQ [6,7] and 6AQ [9] were accomplished by using palladium acetate and copper sulphate solutions in one step. In the each study, the composite materials composed of core (metal)–shell (polymer) hallows were obtained. The copper sulphate is one of the effective oxidizing agents used in organic reactions [11]. In here, methanol solution of copper sulphate was used for oxidizing of AQ. As a result of oxidation reaction, green colored precipitated were obtained with high yield (92%). The general reaction scheme is given in Figure 1.

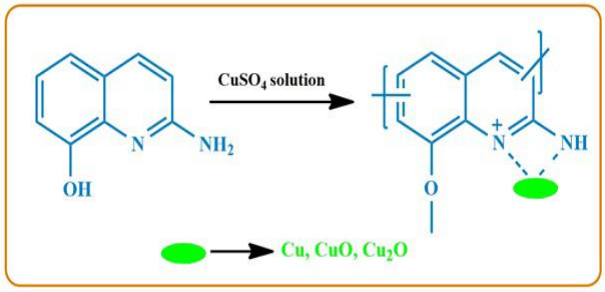

Figure 1. The synthetic procedure for synthesis of AQP/Cu.

The structure and thermal properties of oxidation product were identified by UV-Vis, FTIR, and TG analysis whereas the morphology is revealed by SEM, TEM analysis. SEM images of oxidation product are given in Figure 2.

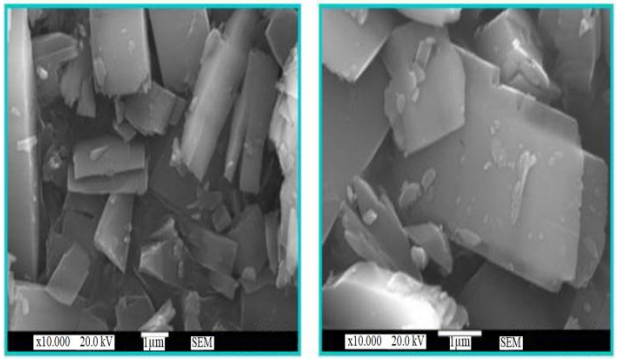

Figure 2. SEM images of AQP/Cu. In the left figure, bar shows 1µm (with 10000 magnifications and in the right figure, bar shows 1µm (with 10000 magnification).

Irregular shaped, heterogeneous and micro-sized plate-like structures were observed from this Figure. EDX analysis assigned the existence of copper, carbon, nitrogen and sulfur atoms on the surface of the product (Figure 3).

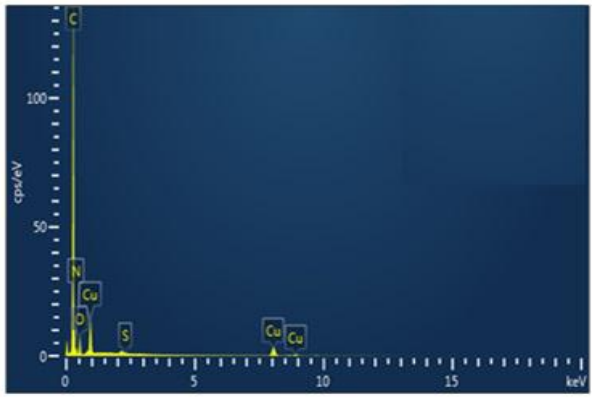

Figure 3. EDX spectrum of AQP/Cu.

TEM images, given in Figure 4, clearly showed that sub-micron copper particles were embedded in the rod like polymer structure.

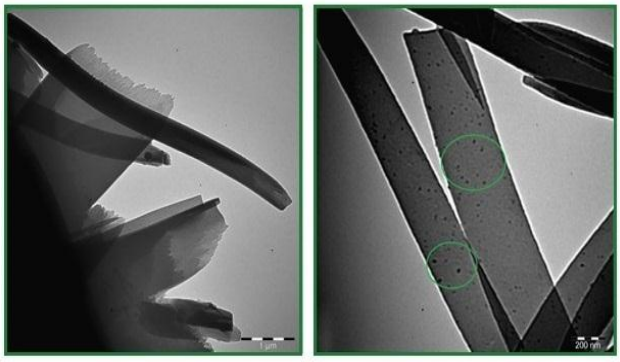

Figure 4. TEM images of AQP/Cu. In the left figure, bar shows 1µm and in the right figure, bar shows 200 nm.

This morphology is different from previous studies [6,7,9]. The thickness and the length of rods observed at Figure 4 were around 200-400 nm, 4-6µm, respectively.

FTIR spectra of resultant and starting material are given in Figure 5.

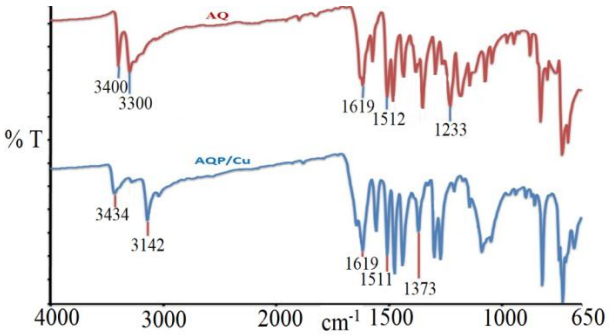

Figure 5. FTIR spectra of AQ and AQP/Cu.

The characteristic benzenoid and quinoid vibrations were observed at 1619 and 1511 cm^{-1}. The peak at 1275 cm^{-1} was also observed possibly due to C-N stretching vibration [7]. In addition, the peak observed at 1373 $cm^{-1}$with medium intensity was assigned to C-N stretching for quinoid ring and harmony with literature [7]. Figure 6 exhibits the UV-Vis spectra of AQ and AQP/Cu in DMSO.

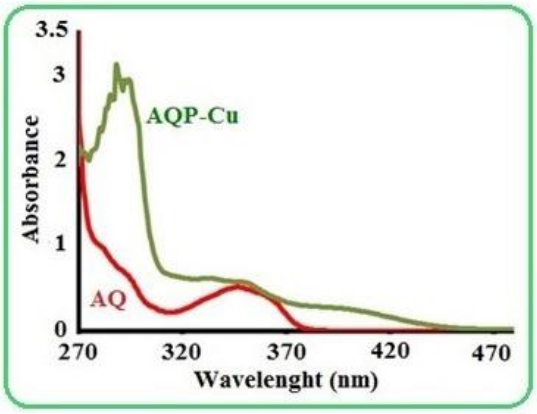

Figure 6. UV-Vis spectra of AQ and AQP/Cu.

One absorption maximum was recorded (at 350 nm) for DMSO solution of AQ. This absorption was attributed to π-π transition. However, AQP/Cu was characterized by three absorption maxima observed at 308, 352 (π-π transitions) and 402 nm (n-π transition). As a result of oxidation reaction, a red-shifted spectrum was recorded for product obtained. An absorption edge around 445 nm was observed for AQP/Cu. The optical band gaps (E_{op}) of AQ and AQP/Cu were measured as given in the literature [12] using $E_{op}=1240/\lambda$ equation and found to be 3.27 and 2.82eV, respectively. As known, the quinoline monomer and polymers exhibit interesting optical properties [2]. Therefore, the fluorescence properties of oxidation product were also studied in here. Figure 7 shows the photographs of AQP/Cu solutions (in toluene and DMSO) recorded under 365 nm UV lamp.

Figure 7. The photographs of AQP/Cu solution in toluene (left) and in DMSO (right). The solution was irritated with UV lamp (365 nm).

As seen from Figure 7, toluene and DMSO solutions of AQP/Cu were blue (turquoise) and purple colored, respectively. The oxidation of 6AQ with copper sulphate solution was accomplished in our previous work and the similar results were obtained [9].The fluorescence spectra of AQP/Cu were obtained in four different solvents (Figure 8).

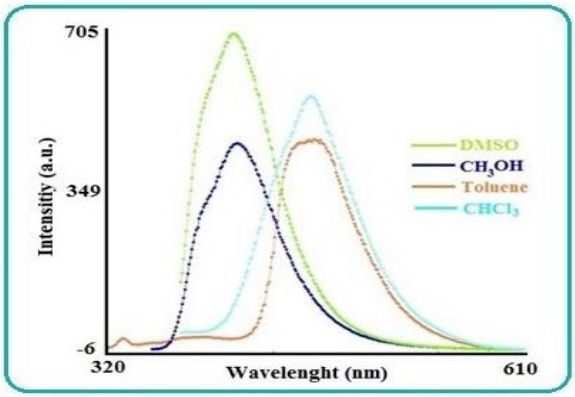

Figure 8. Fluorescence spectra of AQP/Cu recorded in different solvents.

As seen from Figure 8, DMSO and methanol solutions of AQP/Cu exhibited emission maxima about 410 nm as excited at 295 nm. However, in the toluene and chloroform solutions of AQP/Cu exhibited an emission about 470 nm when excited at same wavelength. The solid state conductivity measurements of AQP/Cu were conducted using four-point probe technique. Before measurements, the sample was doped with iodine vapour for 24 hours and the oxidation product exhibited a conductivity value with $8x10^{-9}$ Scm^{-1}.

3.1. Thermal decomposition kinetics of AQP/Cu

In this section of study, thermal decomposition kinetics of AQP/Cu is presented. For a kinetic evaluation, integral conversional methods were used. For determination of kinetic parameters, methods including Flynn-Wall-Ozawa (FWO), Kissinger-Akahira-Sunose (KAS), Tang and also Coats-Redfern (CR) were used. A two-stage decomposition was observed from DTG curve of composite. The temperatures related to the solid state decomposition rates were at 275 (for first decomposition

stage) and 325 ºC (for second decomposition stage). The 20 and 50 % decompositions of AQP/Cu were observed at 265 and 396 ºC, respectively. The residue at 1000º was 29% (for heating rate of 5 ºC min^{-1}). TGA thermograms recorded at heating rates of 5, 10, 15 and 20 ºC min^{-1} are given in Figure 9. TG curves exhibited the similar decomposition character. As seen from this figure, the curves were slightly shifted to right as the heating rates increased.

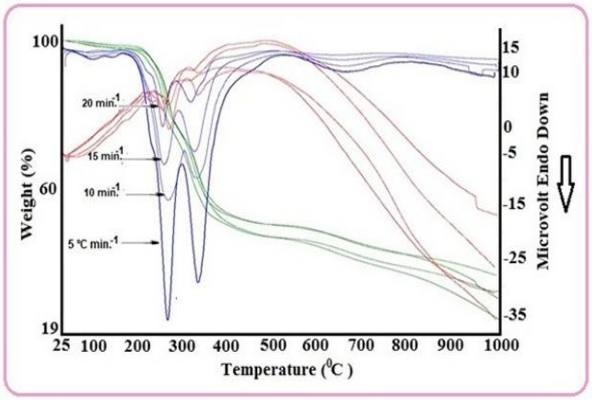

Figure 9. TG-DTG-DTA curves of AQP/Cu obtained in four different heating rates.

Although the apparent kinetic parameters including activation energy, E, and frequency factor A are often determined by nonisothermal methods, International Congress On Thermal Analysis and Calorimetry (ICTAC) purposes the use of the isoconversional methods for calculation of Arrhenius parameters[13]. Therefore, in here, FWO [14,15], Tang [16] and KAS [17,18] procedures were conducted to determine these kinetic parameters. The mathematical equations for these methods (and also for CR [19]) are given in follows:

Tang method

$$\ln[\beta/T^{1.894661}]=\ln[AE/Rg(\alpha)]+3.635011-1.894661\ln E-[1.001450E/RT] \quad \textbf{(3.1)}$$

KAS method

$$\ln[\beta/T^2]=\ln[AE/Rg(\alpha)]-[E/RT] \quad \textbf{(3.2)}$$

FWO method

$$\log\beta=\log[AE/R]-\log g(\alpha)-2.315-0.4567E/RT \quad \textbf{(3.3)}$$

CR method

$$\ln[g(\alpha)/T^2]=\ln[AR/E\beta]-[ERT] \quad \textbf{(3.4)}$$

The terms given in equations 3.1-3.4, are α *(*degree of reaction), g(α) (integral function of conversion), β *(*heating rate), T (DTG peak temperature corresponding maximum decomposition rate) E, activation energy (kJ mol^{-1}), A, pre-exponential factor (s^{-1}) and R gas constant (8.314 kJ mol^{-1}). The first method applied for determination of E parameter (apparent activation energy) is that of Tang. According to this method, E is determined by solution of equation (3.1). E value can be found from a plot of log β versus 1000/T graph. As seen Figure 9, the composite was decomposed in two steps. Therefore, E values were calculated for each decomposition steps and the mean activation energies determined for first and second decomposition steps were 116.6 and 129.9 kJ mol^{-1}, respectively.

The E values determined for each decomposition steps, in 0.05-0.95 conversion range, are given Table 1 and Table 2, respectively.

Table 1. Activation energies determined by KAS, FWO and Tang methods for the first decomposition step of AQP/Cu.

	KAS		Tang		FWO	
α	*E*	*r*	*E*	*r*	*E*	r
0.05	84.50	0.9889	86.36	0.9982	88.86	0.9987
0.1	86.82	0.9983	87.54	0.9894	89.74	0.9993
0.2	124.4	0.9974	125.7	0.9891	126.6	0.9984
0.3	126.3	0.9987	125.5	0.9996	128.5	0.9986
0.4	127.2	0.9977	126.6	0.9991	129.4	0.9971
0.5	128.1	0.9977	127.5	0.9897	129.8	0.9963
0.6	123.7	0.9982	124.6	0.9898	126.3	0.9952
0.7	125.6	0.9963	126.1	0.9896	127.4	0.9956
0.8	127.2	0.9976	126.7	0.9985	128.7	0.9962
0.9	130.4	0.9898	132.3	0.9889	133.6	0.9981
0.95	92.62	0.9899	94.78	0.9987	96.67	0.9987
Mean	116.0		116.6		118.6	

Table 2. Activation energies determined by KAS, FWO and Tang methods for the second decomposition step of AQP/Cu.

	KAS		Tang		FWO	
α	*E*	*r*	*E*	*r*	*E*	*r*
0.05	94.78	0.9878	97.78	0.9783	98.6	0.9882
0.1	103.1	0.9889	106.5	0.9894	108.4	0.9889
0.2	134.6	0.9892	136.4	0.9891	137.8	0.9891
0.3	135.4	0.9994	137.8	0.9897	138.6	0.9892
0.4	134.1	0.9897	138.6	0.9998	139.4	0.9894
0.5	135.8	0.9894	136.7	0.9895	138.7	0.9891
0.6	137.3	0.9893	138.5	0.9891	139.6	0.9891
0.7	133.5	0.9893	135.6	0.9893	137.7	0.9988
0.8	136.6	0.9992	138.1	0.9895	139.7	0.9990
0.9	134.5	0.9988	136.0	0.9983	139.6	0.9982
0.95	126.7	0.9989	127.8	0.9982	129.4	0.9984
Mean	127.8		129.9		131.5	

The second method studied in here is that of KAS. In this method, E is determined by solution of equation (3.2) and obtained from plots of $\ln[\beta/T^2]$ against 1/T graph (for a wide range of conversions). From resulting graph, E values were found to be 116.0 (for first decomposition step) and 127.8 kJ mol^{-1} (for second decomposition step).

The E values determined for each decomposition steps are given Table 1 and Table 2, respectively. The third method applied for determination of E is that of FWO (Eq. 3.3). In this method, E is determined by solution of equation (3.3). From slope of ln β versus 1000/T graph, E values can be determined for different conversions values. E values calculated for first and second decomposition steps were 118.6 and 131.5 kJ mol^{-1}, respectively. E values determined for each decomposition step, in different conversion range, are presented Table 1 and 2, respectively. As seen these results, E values obtained by three different methods are close to each other for different conversion ranges. E values obtained by Tang, KAS and FWO methods were 116.6, 116.0 and 118.6 kJ mol^{-1} (first decomposition step) and 129.9, 127.8 and 131.5 kJ mol^{-1} (second decomposition step), respectively. The last method used in this study is that of CR (equation (3.4)) [19]. CR is a integral method based on single heating rate. Besides kinetic parameters, the thermal decomposition mechanism can be also found using this method. The mathematical functions used in solid state decomposition processes are given in Table 3 [20]. In this method, E values were obtained from solution of Equation 3.4. From slope of ln $[g(\alpha)/T^2]$ against 1000/T graph, E values can be found. E values calculated for a four different heating (5, 10, 15 and 20 °C min^{-1} under a nitrogen atmosphere) for both first and second decomposition steps were presented in Table 4 and Table 5.

Table 3. Mathematical functions used in solid state decomposition processes.

No	Mechanism	Symbol	Differential form, f(α)	Integral form g(α)
Sigmoidal curves				
1	N and G (n=1)	A_1	$(1- \alpha)$	$[-\ln(1- \alpha)]$
2	N and G (n=1.5)	$A_{1.5}$	$(3/2)(1- \alpha)[-\ln(1- \alpha)]^{1/3}$	$[-\ln(1- \alpha)]^{2/3}$
3	N and G (n=2)	A_2	$2(1- \alpha)[-\ln(1- \alpha)]^{1/2}$	$[-\ln(1- \alpha)]^{1/2}$
4	N and G (n=3)	A_3	$3(1- \alpha)[-\ln(1- \alpha)]^{2/3}$	$[-\ln(1- \alpha)]^{1/3}$
5	N and G (n=4)	A_4	$4(1- \alpha)[-\ln(1- \alpha)]^{3/4}$	$[-\ln(1- \alpha)]^{1/4}$
Deceleration curves				
6	Diffusion, 1D	D_1	$1/(2\alpha)$	α^2
7	Diffusion, 2D	D_2	$1/(\ln(1- \alpha))$	$(1- \alpha)\ln(1- \alpha)+ \alpha$
8	Diffusion, 3D	D_3	$1.5/[(1- \alpha)^{-1/3}-1]$	$(1-2\alpha/3)-(1- \alpha)^{2/3}$
9	Diffusion, 3D	D_4	$[1.5(1- \alpha)^{2/3}][1-(1- \alpha)^{1/3}]^{-1}$	$[1-(1- \alpha)^{1/3}]^2$
10	Diffusion, 3D	D_5	$(3/2)(1+ \alpha)^{2/3}[(1+ \alpha)^{1/3}-1]^{-1}$	$[(1+ \alpha)^{1/3}-1]^2$
11	Diffusion, 3D	D_6	$(3/2)(1- \alpha)^{4/3}[[1/(1- \alpha)^{1/3}]-1]^{-1}$	$[[1/(1- \alpha)]^{1/3}-1]^2$
12	Contracted geometry shape (cylindrical symmetry)	R_2	$3(1- \alpha)^{2/3}$	$1-(1- \alpha)^{1/3}$
13	Contracted geometry shape (sphere symmetry)	R_3	$3(1- \alpha)^{2/3}$	$1-(1- \alpha)^{1/3}$
Acceleration curves				
14	Mample power law	P_1	1	A
15	Mample power law (n=2)	P_2	$2\alpha^{½}$	$\alpha^{1/2}$
16	Mample power law (n=3)	P_3	$(1.5)\alpha^{2/3}$	$\alpha^{1/3}$
17	Mample power law (n=4)	P_4	$4\alpha^{¾}$	$\alpha^{¼}$
18	Mample power law (n=2/3)	$P_{3/2}$	$2/3(\alpha)^{-1/2}$	$\alpha^{3/2}$
19	Mample power law (n=3/2)	$P_{2/3}$	$3/2(\alpha)^{1/3}$	$\alpha^{2/3}$
20	Mample power law (n=4/3)	$P_{3/4}$	$4/3(\alpha)^{-1/3}$	$\alpha^{3/4}$

Table 4 .The activation energies obtained for the first decomposition step of AQP/Cu by the CR method in the nitrogen atmosphere.

	5 °C min^{-1}		10 °C min^{-1}		15 °C min^{-1}		20 °C min^{-1}	
	E (kJ mol^{-1})	*r*	*E* (kJ mol^{-1})	*r*	*E* (kJ mol^{-1})	*r*	*E* (kJ mol^{-1})	*r*
A_1	50.6	0.96784	52.2	0.96878	52.6	0.96788	53.6	0.96886
$A_{1,5}$	48.0	0,96766	49.4	0,96676	49.6	0,96777	40.6	0,96677
A_2	26.6	0.98327	28.4	0.98632	29.0	0.98374	29.4	0.97831
A_3	15.8	0.97845	15.	0.97864	16.1	0.97881	17.7	0.97786
A_4	20.2	0.98878	21.6	0.98876	21.0	0.98817	22.6	0.97888
D_1	80.9	0.97881	81.6	0.97687	82.5	0.97881	83.0	0.98787

D_2	100.	0.98924	102.9	0.98692	104.7	0.98971	105.6	0.97890
D_3	115.2	0.97927	114.2	0.97692	114.9	0.97911	115.8	0.98791
D_4	122.5	0.98886	122.1	0.98688	124.8	0.98886	124.3	0.97881
D_5	92.7	0.98917	93.4	0.98791	93.7	0.98964	94.6	0.98892
D_6	143.8	0.98966	144.5	0.98696	145.2	0.98912	143.5	0.98896
R_2	56.0	0.98878	56.2	0.98887	57.4	0.98874	57.9	0.98886
R_3	63.9	0.98729	64.4	0.98872	65.0	0.98786	65.6	0.97877
P_1	51.1	0.97887	52.5	0.97888	52.2	0.97888	53.1	0.97781
P_2	27.8	0.98851	27.8	0.98885	28.2	0.98842	18.2	0.98880
P_3	10.6	0.98840	10.6	0.98884	10.6	0.98878	10.4	0.98887
P_4	6.6	0.97820	6.5	0.97882	6.6	0.97876	6.6	0.98781
$P_{3/2}$	76.8	0.98862	77.1	0.98986	77.8	0.98861	78.8	0.98888
$P_{2/3}$	45.9	0.97854	46.1	0.97784	46.6	0.97887	46.4	0.98782
$P_{3/4}$	59.7	0.96876	50.2	0.96786	50.6	0.9686	50.6	0.97681

Table 5 . The activation energies obtained for the second decomposition step of AQP/Cu by the CR method in the nitrogen atmosphere.

	5 °C min^{-1}		10 °C min^{-1}		15 °C min^{-1}		20 °C min^{-1}	
	E (kJ mol^{-1})	*r*	*E* (kJ mol^{-1})	*r*	*E* (kJ mol^{-1})	*r*	*E* (kJ mol^{-1})	*r*
A_1	44.0	0.98834	41.1	0.99812	43.6	0.99843	43.8	0.99842
$A_{1,5}$	29.1	0.98845	28.2	0.98813	29.4	0.98965	28.6	0.98932
A_2	22.4	0.98687	22.6	0.98775	22.7	0.98592	27.2	0.98597
A_3	15.2	0.98658	14.1	0.98336	14.9	0.98579	14.4	0.98429
A_4	2.7	0.99895	2.1	0.99811	2.2	0.98854	2.3	0.98872
D_1	90.1	0.98886	90.6	0.98960	91.7	0.98841	90.8	0.98834
D_2	108.9	0.98789	108.9	0.98897	109.4	0.98083	108.7	0.98685
D_3	111.8	0.98767	112.5	0.98129	112.6	0.98788	112.8	0.98228
D_4	127.7	0.98848	128.9	0.98801	128.0	0.98854	127.7	0.97874
D_5	146.2	0.99818	147.5	0.99822	147.7	0.99823	148.2	0.98775
D_6	158.8	0.99371	158.9	0.99482	159.2	0.99683	159.6	0.99578
R_2	46.9	0.98797	47.0	0.98418	47.2	0.98718	64.4	0.98472
R_3	49.7	0.98883	50.1	0.97845	50.2	0.9823	50.5	0.98767
P_1	21.0	0.98768	21.0	0.98765	22.6	0.97711	22.2	0.98776
P_2	15.1	0.98579	15.1	0.98276	16.1	0.98743	17.1	0.98787
P_3	10.7	0.98447	11.7	0.98437	12.4	0.98273	12.7	0.98874
P_4	12.0	0.98821	12.4	0.98865	12.6	0.98247	12.8	0.98680
$P_{3/2}$	46.7	0.98862	47.2	0.98813	47.4	0.97977	48.6	0.98768
$P_{2/3}$	20.6	0.98574	21.7	0.98482	22.7	0.98832	22.8	0.98883
$P_{3/4}$	23.4	0.98776	23.6	0.98148	23.4	0.98564	23.8	0.98787

From these data, it was found that the most suitable decomposition mechanism for the first decomposition step of composite (20 °C min^{-1}) was D_3. However, D_4 was determined as the most suitable mechanism for the second decomposition step (10 °C min^{-1}).

4. Conclusion

The results of this study showed that the copper sulphate solution could effectively oxidize AQ in ambient conditions. As a result of oxidation reaction, a composite product composed of quinoline polymer and copper particles was obtained. TEM images assigned that sub-micron copper particles were dispersed on the rod like polymer structure. The composite was decomposed in two main decomposition steps. These decomposition steps were kinetically analyzed. For a kinetic evaluation, FWO, KAS, Tang and CR methods were used. E values obtained by Tang, KAS and FWO method were found to be 116.6, 116.0, and 118.6 kJ mol^{-1} for first decomposition stage and 129.9, 127.8 and 131.5 kJ mol^{-1} for the second decomposition stage, respectively. For determination of decomposition mechanism of composite, CR method was also studied and Dn type mechanism was suggested for each decomposition step.

Acknowledgements

This study is financially supported by Çanakkale Onsekiz Mart University Scientific Research Project Coordination Unit (Project number: FBA-2014-288).

References

1. Stille, J.K, Polyquinolines, *Macromolecules*, 1981, 14(3), 870–880.

2. Kimyonok, A, Wang, X.Y, Weck, M, Electroluminescent poly(quinoline)s and metalloquinolates, *Journal Macromolecular Science Part C Polymer Reviews*, 2006, 46 (1), 47-77.

3. Thivaios, I, Koukoumtzis, V, Kallitsis, J.K, Bokias, G, Quinoline-labeled poly(N-isopropylacrylamide): a selective polymeric luminescent sensor of cationic surfactants, *Sensors and Actuators B*, 2016, 233, 127-135.

4. Bilici, A, Chemical oxidation of 5-amino quinoline with $(NH_4)_2S_2O_8$: synthesis and characterization, *Hacettepe Journal of Biology and Chemistry*, 2017, 45, 563-571.

5. Yu, L, Han, Z, Ding, Y, Gram-scale preparation of Pd@PANI: a practical catalyst reagent for copper-free and ligand-free Sonogashira couplings, *Organic Process Research & Development*, 2016, 20 (12), 2124−2129.

6. Islam, R.U, Mahato, S.K, Shukla, S.K, Witcomb, M.J, Mallick, K, Palladium–poly(3-aminoquinoline) hollow-sphere composite: application in Sonogashira coupling reactions, *ChemCatChem*, 2013, 5 (8), 2453–2461

7. Choudhary, M, Islam, R.U, Witcom, M.J, Phali, M, Mallick, K, Template-less synthesis of polymer hollow spheres: an efficient catalyst for Suzuki coupling reaction, *Applied Organometallic Chemistry*, 2013, 27 (9), 523–528.

8. Bilici, A, Ayten, B, Kaya, İ, Facile preparation of gold nanoparticles on the polyquinoline matrix: catalytic performance toward 4-nitrophenol reduction, Synthetic *Metals*, 2015, 201, 11-17.

9. Bilici, A, Tezel, R.N, Kaya, İ, Facile chemical route to copper/polymer composite: simultaneous reduction and polymerization, *Colloids and Surfaces A: Physicochemical and Engineering Aspects*, 2014, 459 (5), 254-260.

10. Mallick, K, Witcomb, M.J, Scurrell, M.S, In situ synthesis of copper nanoparticles and poly(o-toluidine): a metal–polymer composite material, *European Polymer Journal*, 2006, 42(3) , 670-675.

11. Islam, R.U., Taher, A., Choudhary, M., Siwal, S., Mallick K., Polymer immobilized Cu(I) formation and azide-alkyne cycloaddition: A one pot reaction, *Scientific Reports*, 2015, 5, 1-8.

12. Costa, J.C.S, Taveira, R.J.S, Lima, C.F.R.A.C, Mendes, A, Santos, L.M.N.B.F, Optical band gaps of organic semiconductor materials, *Optical Materials*, 2016, 58, 51–60.

13. Vyazovkin, S, Burnham, A.K, Criado, J.M, Pérez-Maqueda, L.A, Popescu C, Sbirrazzuoli, N, ICTAC kinetics committee recommendations for performing kinetic computations on thermal analysis data, *Thermochimica Acta*, 2011, 520, 1-19.

14. Flynn, J.H, Wall, L.A, A quick, direct method for the determination of activation energy from thermogravimetric data, *Journal of Polymer Science Part C: Polymer Letters*, 1966, 4 (5), 323–328.

15. Takeo, O, A new method of analyzing thermogravimetric data., *Bulletin of the Chemical Society of Japan*, 1965, 38 (11), 1881–1886

16. Wanjun, T, Yuwen, L, Xi Y, Cunxin, W, Kinetic studies of the calcination of ammonium metavanadate by thermal methods, *Industrial & Engineering Chemistry Research*, 2004, 43 (9), 2054–2059.

17. Kissinger, H.E, Reaction kinetics in differential thermal analysis, *Analytical Chemistry*, 1957, 29 (11), 1702–1706.

18. Akahira, T, Sunose, T, Method of determining activation deterioration constant of electrical insulating materials, *Research Report Chiba Institute of Technology*, 1971, 16, 22–31.

19. Coats, A.W, Redfern, J.P, Kinetics parameters from thermogravimetric data. *Nature*, 1964, 201, 68-69.

20. Kamel, L.T, The kinetic analysis of non- isothermal carisoprodol reaction in nitrogen atmosphere using the invariant kinetic parameters method, *European Journal of Chemistry*, 2014, 5 (3), 507- 512.